

Hamiltonian of a flux qubit-LC oscillator circuit in the deep-strong-coupling regime

F. Yoshihara,^{1,*} S. Ashhab,² T. Fuse,¹ M. Bamba,^{3,4} and K. Semb¹

¹*Advanced ICT Institute, National Institute of Information and Communications Technology,
4-2-1, Nukuikitamachi, Koganei, Tokyo 184-8795, Japan*

²*Qatar Environment and Energy Research Institute,
Hamad Bin Khalifa University, Qatar Foundation, Doha, Qatar*

³*Department of Physics, Kyoto University, Kyoto 606-8502, Japan*

⁴*PRESTO, Japan Science and Technology Agency, Kawaguchi 332-0012, Japan*

(Dated: December 22, 2024)

We derive the Hamiltonian of a superconducting circuit that comprises a single-Josephson-junction flux qubit and an LC oscillator. If we keep the qubit's lowest two energy levels, the derived circuit Hamiltonian takes the form of the quantum Rabi Hamiltonian, which describes a two-level system coupled to a harmonic oscillator, regardless of the coupling strength. To investigate contributions from the qubit's higher energy levels, we numerically calculate the transition frequencies of the circuit Hamiltonian. We find that the qubit's higher energy levels mainly cause an overall shift of the entire spectrum, but the energy level structure up to the seventh excited states can still be fitted well by the quantum Rabi Hamiltonian even in the case where the coupling strength is larger than the frequencies of the qubit and the oscillator, i.e., when the qubit-oscillator circuit is in the deep-strong-coupling regime. We also confirm that some of the paradoxical properties of the quantum Rabi Hamiltonian in the deep-strong-coupling regime, e.g. the non-negligible number of photons and the nonzero expectation value of the flux in the oscillator in the ground state, arise from the circuit Hamiltonian as well.

Superconducting circuits are one of the most promising platforms for realizing large-scale quantum information processing. One of the most important features of superconducting circuits is the freedom they allow in their circuit design. Since the first demonstration of the coherent control of a Cooper pair box [1], various types of superconducting circuits have been demonstrated. In principle, the Hamiltonian of a superconducting circuit can be derived using the standard quantization procedure applied to the charge and flux variables in the circuit [2]. The Hamiltonian of an LC oscillator is well known to be that of a harmonic oscillator. The Hamiltonians of various kinds of superconducting qubits have also been well studied [3–7] and these Hamiltonians can be numerically diagonalized to obtain eigenenergies and eigenstates that accurately reproduce experimental data. On the other hand, the Hamiltonian of circuits consisting of two or more components, i.e., qubit-qubit, qubit-oscillator, or oscillator-oscillator systems, are usually treated in such a way that the Hamiltonian of the individual components and the coupling among them are separately obtained [8–11]. This separate treatment of individual circuit components works reasonably well in most circuits. Even for flux qubit-oscillator circuits in the ultrastrong-coupling [12, 13] regime, where the coupling strength g is around 10% of the oscillator's frequency ω and the qubit frequency Δ_q , or the deep-strong-coupling [14–16] regime, where g is comparable to or larger than Δ_q and ω , the experimental data can be well fitted by the quantum Rabi Hamiltonian [17–19], where a two-level atom and a harmonic oscillator are coupled by a dipole-dipole

interaction. However, the more rigorous approach based on the standard quantization procedure has not been applied to such circuits except in a few specific studies [20–22], and the validity of describing a flux qubit-oscillator circuit by the quantum Rabi Hamiltonian has not been demonstrated from this perspective.

In this paper, we apply the standard quantization procedure to a superconducting circuit in which a single-Josephson-junction flux qubit (an rf-SQUID qubit or an equivalent circuit of a fluxonium) and an LC oscillator are inductively coupled to each other by sharing an inductor [Fig. 1(a)], and derive the Hamiltonian of the circuit. Note that single-Josephson-junction flux qubits have been experimentally demonstrated using superconductors, realized by high-kinetic-inductance superconductors [23, 24], granular aluminum [25], and Josephson-junction arrays [26]. The derived circuit Hamiltonian consists of terms associated with the LC oscillator, the flux qubit (and its higher energy levels), and the product of the two flux operators. Excluding the qubit's energy levels higher than the first excited state, this circuit Hamiltonian takes the form of the quantum Rabi Hamiltonian. To investigate contributions from the qubit's higher energy levels, we numerically calculate the transition frequencies of the circuit Hamiltonian. We find that the qubit's higher energy levels mainly cause a negative shift of the entire spectrum, and that the calculated transition frequencies are well fitted by the quantum Rabi Hamiltonian even when the qubit-oscillator circuit is in the deep-strong-coupling regime. Using the circuit Hamiltonian, we investigate some of the paradoxical properties of the quantum Rabi Hamiltonian in the deep-strong-coupling regime, the non-negligible number of photons and the nonzero expectation value of the flux

* fumiki@nict.go.jp

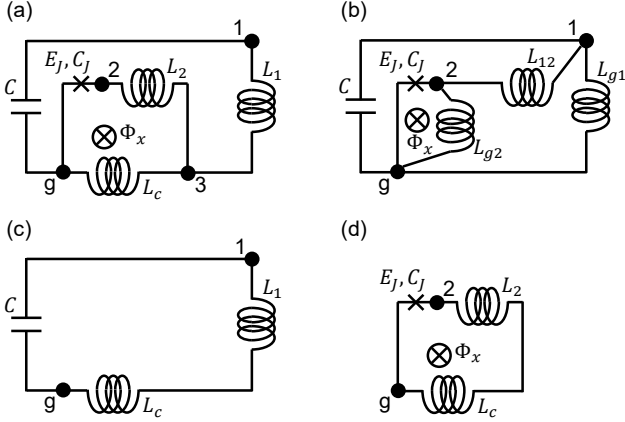


FIG. 1. Circuit diagrams. (a) A superconducting circuit in which a single-Josephson-junction flux qubit and an LC oscillator are inductively coupled to each other by sharing an inductor. (b) Equivalent circuit of (a) obtained by applying the so-called star-delta (Y- Δ) transformation to the inductor network in circuit (a). (c) The outer loop of circuit (a), which forms an LC oscillator. (d) The inner loop of circuit (a), which forms a single-Josephson-junction flux qubit.

in the oscillator in the ground state [27]. Note that although the expectation value of the flux in the oscillator is nonzero, the expectation value of the current is zero, meaning that an unphysical DC current through the inductor of an LC oscillator is not predicted.

Following the standard quantization procedure, nodes are assigned to the circuit as shown in Fig. 1(a). Before deriving the circuit Hamiltonian, the circuit in Fig. 1(a) is transformed to the one shown in Fig. 1(b) by applying the so-called star-delta (Y- Δ) transformation to the inductor network. Then, node 3 surrounded by the inductors can be removed. The inductances of the new set of inductors are given as $L_{g1} = (L_c L_1 + L_c L_2 + L_1 L_2) / L_2$, $L_{g2} = (L_c L_1 + L_c L_2 + L_1 L_2) / L_1$, and $L_{12} = (L_c L_1 + L_c L_2 + L_1 L_2) / L_c$.

The Lagrangian of the circuit can now be obtained relatively easily:

$$\hat{\mathcal{L}}_{circ} = \frac{C}{2} \dot{\hat{\Phi}}_1^2 + \frac{C_J}{2} \dot{\hat{\Phi}}_2^2 + E_J \cos \left(2\pi \frac{\hat{\Phi}_2 - \Phi_x}{\Phi_0} \right) - \frac{\hat{\Phi}_1^2}{2L_{g1}} - \frac{\hat{\Phi}_2^2}{2L_{g2}} - \frac{(\hat{\Phi}_2 - \hat{\Phi}_1)^2}{2L_{12}}, \quad (1)$$

where C_J and $E_J = I_c \Phi_0 / (2\pi)$ are the capacitance and the Josephson energy of the Josephson junction, I_c is the critical current of the Josephson junction, $\Phi_0 = h/(2e)$ is the superconducting flux quantum, and $\hat{\Phi}_k$ and $\dot{\hat{\Phi}}_k$ ($k = 1, 2$) are the node flux and its time derivative for node k . The node charges are defined as the conjugate momenta of the node fluxes as $\hat{q}_k = \partial \hat{\mathcal{L}}_{circ} / \partial \dot{\hat{\Phi}}_k$. After the Legendre transformation, the Hamiltonian is ob-

tained as

$$\begin{aligned} \hat{\mathcal{H}}_{circ} &= \frac{\hat{q}_1^2}{2C} + \frac{\hat{q}_2^2}{2C_J} - E_J \cos \left(2\pi \frac{\hat{\Phi}_2 - \Phi_x}{\Phi_0} \right) \\ &\quad + \frac{\hat{\Phi}_1^2}{2L_{LC}} + \frac{\hat{\Phi}_2^2}{2L_{FQ}} - \frac{\hat{\Phi}_1 \hat{\Phi}_2}{L_{12}} \\ &= \hat{\mathcal{H}}_1 + \hat{\mathcal{H}}_2 + \hat{\mathcal{H}}_{12}, \end{aligned} \quad (2)$$

where

$$\hat{\mathcal{H}}_1 = \frac{\hat{q}_1^2}{2C} + \frac{\hat{\Phi}_1^2}{2L_{LC}}, \quad (3)$$

$$\hat{\mathcal{H}}_2 = \frac{\hat{q}_2^2}{2C_J} - E_J \cos \left(2\pi \frac{\hat{\Phi}_2 - \Phi_x}{\Phi_0} \right) + \frac{\hat{\Phi}_2^2}{2L_{FQ}}, \quad (4)$$

$$\hat{\mathcal{H}}_{12} = -\frac{\hat{\Phi}_1 \hat{\Phi}_2}{L_{12}}, \quad (5)$$

$$L_{LC}^{-1} = L_{g1}^{-1} + L_{12}^{-1}, \text{ and } L_{FQ}^{-1} = L_{g2}^{-1} + L_{12}^{-1}.$$

As can be seen from Eq. (2), the Hamiltonian $\hat{\mathcal{H}}_{circ}$ can be separated into three parts: the first part $\hat{\mathcal{H}}_1$ consisting of the charge and flux operators of node 1, the second part $\hat{\mathcal{H}}_2$ consisting of node 2 operators, and the third part $\hat{\mathcal{H}}_{12}$ containing the product of the two flux operators. Let us consider a separate treatment of the circuit shown in Fig. 1(a), where the circuit is assumed to be naively divided into the two coupled components. The capacitor and the inductors in the outer loop of the circuit in Fig. 1(a) form an LC oscillator [Fig. 1(c)]. The Josephson junction and the inductors in the inner loop form a single-Josephson-junction flux qubit [Fig. 1(d)]. The LC oscillator and the single-Josephson-junction flux qubit share the inductor L_c at the common part of the two loops. It is instructive to investigate the relation of the following pairs of Hamiltonians: $\hat{\mathcal{H}}_1$ and the Hamiltonian of the LC oscillator shown in Fig. 1(c), $\hat{\mathcal{H}}_2$ and the Hamiltonian of the flux qubit shown in Fig. 1(d), and $\hat{\mathcal{H}}_{12}$ and the Hamiltonian of the inductive coupling between the LC oscillator and the flux qubit $M \hat{I}_{LC} \hat{I}_q = -L_c / [(L_c + L_1)(L_c + L_2)] \hat{\Phi}_1 \hat{\Phi}_2$, where we have used the relations of the oscillator current $\hat{I}_{LC} = \hat{\Phi}_1 / (L_c + L_1)$, the qubit current $\hat{I}_q = \hat{\Phi}_2 / (L_c + L_2)$, and the mutual inductance $M = L_c$. Actually, only the inductances are different in the Hamiltonians of the two pictures: The inductances of the LC oscillator, the flux qubit, and the coupling Hamiltonians derived from the separate treatment are respectively $L_c + L_1$, $L_c + L_2$, and $-(L_c + L_1)(L_c + L_2) / L_c$, while those in $\hat{\mathcal{H}}_{circ}$ are L_{LC} , L_{FQ} , and $-L_{12}$. Figure 2 shows the inductances in the separate treatment and in $\hat{\mathcal{H}}_{circ}$ as functions of L_c on condition that the inductance sums are kept constant at $L_c + L_1 = 800$ pH and $L_c + L_2 = 2050$ pH. As L_c approaches 0, $L_c + L_1 \rightarrow L_{LC}$, $L_c + L_2 \rightarrow L_{FQ}$, and $(L_c + L_1)(L_c + L_2) / L_c \rightarrow L_{12}$. In this way, the Hamiltonian derived from the separate treatment has the same

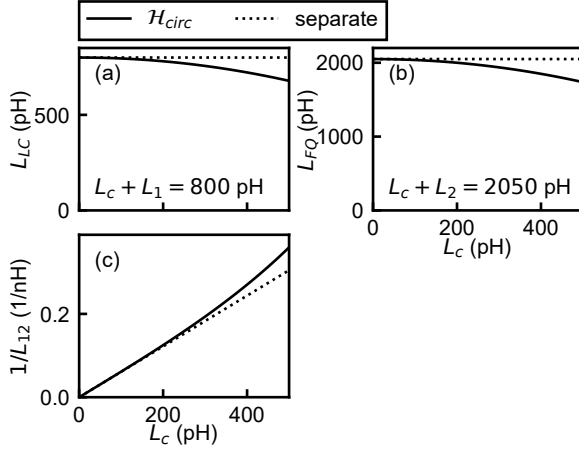


FIG. 2. (a), (b), (c) The inductances of the LC oscillator L_{LC} , the flux qubit L_{FQ} , and the inverse inductance of $\hat{\mathcal{H}}_{12}$, $1/L_{12}$, (solid lines) are plotted as functions of L_c together with their counterparts in the separate treatment (dotted lines) on condition that the inductance sums are kept constant at $L_c + L_1 = 800$ pH and $L_c + L_2 = 2050$ pH.

form as $\hat{\mathcal{H}}_{circ}$, and the inductances in the separate treatment approach those of $\hat{\mathcal{H}}_{circ}$ in the case $L_c \ll L_1, L_2$.

Next, we compare the Hamiltonian $\hat{\mathcal{H}}_{circ}$ with the generalized quantum Rabi Hamiltonian:

$$\begin{aligned} \hat{\mathcal{H}}_R/\hbar &= \omega \left(\hat{a}^\dagger \hat{a} + \frac{1}{2} \right) - \frac{1}{2} (\varepsilon \hat{\sigma}_x + \Delta_q \hat{\sigma}_z) \\ &\quad + g \hat{\sigma}_x (\hat{a} + \hat{a}^\dagger) \\ &= \left(\hat{\mathcal{H}}_{LC} + \hat{\mathcal{H}}_{FQ} + \hat{\mathcal{H}}_{coup} \right) / \hbar. \end{aligned} \quad (6)$$

The first part $\hat{\mathcal{H}}_{LC}$ represents the energy of the LC oscillator, where \hat{a}^\dagger and \hat{a} are the creation and annihilation operators, respectively. The second part $\hat{\mathcal{H}}_{FQ}$ represents the energy of the flux qubit written in the energy eigenbasis at $\varepsilon = 0$. The operators $\hat{\sigma}_{x,z}$ are the standard Pauli operators. The parameters $\hbar \Delta_q$ and $\hbar \varepsilon$ are the tunnel splitting and the energy bias between the two states with persistent currents flowing in opposite directions around the qubit loop. The third part $\hat{\mathcal{H}}_{coup}$ represents the coupling energy.

The relation between $\hat{\mathcal{H}}_1$ and $\hat{\mathcal{H}}_{LC}$ is straightforward. The resonance frequency and the operators in $\hat{\mathcal{H}}_{LC}$ can be analytically described by the variables and operators in $\hat{\mathcal{H}}_1$ as $\omega = 1/\sqrt{L_{LC}C}$ and $\hat{a} + \hat{a}^\dagger \rightarrow \hat{\Phi}_1/(L_{LC}I_{zpf})$, where $I_{zpf} = \sqrt{\hbar\omega/(2L_{LC})}$ is the zero-point-fluctuation current. To see the relation between $\hat{\mathcal{H}}_2$ and $\hat{\mathcal{H}}_{FQ}$, we numerically calculated the eigenenergies of $\hat{\mathcal{H}}_2$ as functions of Φ_x . In the calculation, we use the following parameters: $L_c + L_2 = 2050$ pH, $E_J/h = 165.1$ GHz ($L_J = 990$ pH), and $C_J = 4.84$ fF ($E_C/h = 4.0$ GHz). As shown in Fig. 3(a) the lowest two energy levels are isolated from the higher levels, which are more than 40 GHz

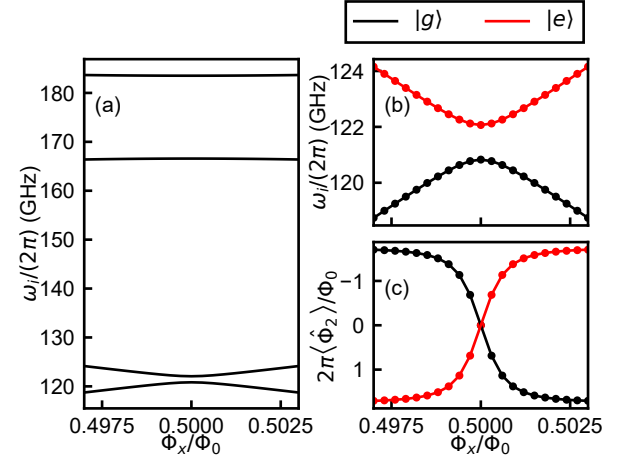


FIG. 3. (a) Numerically calculated energy levels of $\hat{\mathcal{H}}_2$ as functions of Φ_x . (b) The lowest two energy levels of $\hat{\mathcal{H}}_2$. (c) The expectation values of the flux operator $\langle g | \hat{\Phi}_2 | g \rangle$ and $\langle e | \hat{\Phi}_2 | e \rangle$. The solid circles are obtained from numerical calculations of $\hat{\mathcal{H}}_2$, while the lines are obtained from fitting by $\hat{\mathcal{H}}_{FQ}$. The black and red colors respectively indicate states $|g\rangle$ and $|e\rangle$. In the calculation, we use the following parameters: $L_c + L_2 = 2050$ pH, $E_J/h = 165.1$ GHz ($L_J = 990$ pH), and $C_J = 4.84$ fF ($E_C/h = 4.0$ GHz).

higher in frequency. The lowest two energy levels of $\hat{\mathcal{H}}_2$ are well fitted by $\hat{\mathcal{H}}_{FQ}$ [Fig. 3(b)]. Besides the offset in the y axis, the fitting parameters are Δ_q and the maximum persistent current I_p , which is determined as the proportionality constant between the energy bias and the flux bias, $\varepsilon = 2I_p(\Phi_x - 0.5\Phi_0)$. We also numerically calculated the expectation values of the flux operator, $\langle g | \hat{\Phi}_2 | g \rangle$ and $\langle e | \hat{\Phi}_2 | e \rangle$, which are well fitted by $\langle g | \hat{\sigma}_x | g \rangle$ and $\langle e | \hat{\sigma}_x | e \rangle$, respectively [Fig. 3(c)]. Here, $|g\rangle$ and $|e\rangle$ are respectively the ground and excited states of the qubit. The only fitting parameter is determined by the ratio $\Phi_{2max} = -\langle i | \hat{\Phi}_2 | i \rangle / \langle i | \hat{\sigma}_x | i \rangle$ ($i = g, e$). Now, the Pauli operator $\hat{\sigma}_x$ is identified as being proportional to the flux operator $\hat{\sigma}_x \rightarrow -\hat{\Phi}_2/\Phi_{2max}$. The relation between $\hat{\mathcal{H}}_{12}$ and $\hat{\mathcal{H}}_{coup}$ can now be obtained by using the relations for the oscillator and qubit operators identified above. This way we find that the Hamiltonian $\hat{\mathcal{H}}_{12}$ can be described as $-(L_{LC}/L_{12})I_{zpf}\Phi_{2max}\hat{\sigma}_x(\hat{a} + \hat{a}^\dagger)$, which is exactly the same form as $\hat{\mathcal{H}}_{coup}$, with the coupling strength $\hbar g = -(L_{LC}/L_{12})I_{zpf}\Phi_{2max}$. Note that $\hat{\mathcal{H}}_{coup}$ is derived in the flux gauge, which is optimal for our system with the single oscillator mode [28–30]. Excluding the qubit's energy levels higher than the first excited states, $\hat{\mathcal{H}}_{circ}$ takes the form of $\hat{\mathcal{H}}_R$. In other words, once the circuit parameters, i.e. Φ_x , L_c , L_1 , L_2 , C , E_J , and C_J , are given, the corresponding parameters in $\hat{\mathcal{H}}_R$ (ω , ε , Δ_q , and g) are obtained. The relation between $\hat{\mathcal{H}}_{circ}$ and $\hat{\mathcal{H}}_R$ is summarized in Table I.

$\hat{\mathcal{H}}_R$	$\hat{\mathcal{H}}_{circ}$
$\hat{\mathcal{H}}_{LC}$	$\hat{\mathcal{H}}_1$
$\hat{\mathcal{H}}_{FQ}$	$\hat{\mathcal{H}}_2$
$\hat{\mathcal{H}}_{coup}$	$\hat{\mathcal{H}}_{12}$
$\hat{a} + \hat{a}^\dagger$	$\hat{\Phi}_1/(L_{LC}I_{zpf})$
$(\hat{a} - \hat{a}^\dagger)/i$	$\hat{q}_1/(CV_{zpf})$
$\hat{\sigma}_x$	$-\hat{\Phi}_2/\Phi_{2max}$
$\hat{\sigma}_z$	—
ω	$1/\sqrt{L_{LC}C}$
ε	$2I_p(\Phi_x - 0.5\Phi_0)$
Δ_q	Δ_q
g	$(L_{LC}/L_{12})I_{zpf}\Phi_{2max}/\hbar$

TABLE I. Hamiltonians, operators, and variables in $\hat{\mathcal{H}}_R$ and their counterparts in $\hat{\mathcal{H}}_{circ}$. $I_{zpf} = \sqrt{\hbar\omega/(2L_{LC})}$ and $V_{zpf} = \sqrt{\hbar\omega/(2C)}$ are the zero-point-fluctuation current and voltage, respectively. The parameters Φ_{2max} , I_p , and Δ_q are obtained by numerically calculating the eigenenergies of $\hat{\mathcal{H}}_2$ as functions of Φ_x and fitting the lowest two energy levels by $\hat{\mathcal{H}}_{FQ}$. Note that there is no analytic expression of $\hat{\sigma}_z$ and Δ_q .

As previously mentioned, $\hat{\mathcal{H}}_R$ considers only the lowest two energy levels of the flux qubit, while $\hat{\mathcal{H}}_{circ}$ includes all energy levels. To investigate the effect of the qubit's higher energy levels, we perform numerical calculations and compare the energy levels calculated by $\hat{\mathcal{H}}_R$ and $\hat{\mathcal{H}}_{circ}$. The details of the numerical diagonalization of $\hat{\mathcal{H}}_{circ}$ are given in Appendix A. Since the contributions from the qubit's higher energy levels are expected to become larger as the coupling strength increases, the numerical calculations cover a wide range of coupling strengths from the weak-coupling to the deep-strong-coupling regime. In the calculation, we fix $L_c + L_1 = 800$ pH, $L_c + L_2 = 2050$ pH, $C = 0.87$ pF, $E_J/h = 165.1$ GHz ($L_J = 990$ pH), and $C_J = 4.84$ fF ($E_C/h = 4.0$ GHz), and sweep the flux bias Φ_x around $\Phi_0/2$ at various values of L_c . Some of our calculations were performed using the QuTiP simulation package [31].

Transition frequencies of the qubit-oscillator circuit ω_{ij} corresponding to the transition $|i\rangle \rightarrow |j\rangle$ numerically calculated from $\hat{\mathcal{H}}_{circ}$ around the resonance frequency of the oscillator ω are plotted in Fig. 4 for (a) $L_c = 20$ pH and (b) $L_c = 350$ pH, where the indices i and j label the energy eigenstates according to their order in the energy-level ladder, with the index 0 denoting the ground state. In the case $L_c = 20$ pH, the spectrum indicates that the qubit and the oscillator are strongly coupled. Around $\Phi_x/\Phi_0 = 0.5$, a dispersive shift of the oscillator frequency is observed. Note that transitions $|0\rangle \rightarrow |2\rangle$ and $|1\rangle \rightarrow |3\rangle$ around $\Phi_x/\Phi_0 = 0.5$ respectively correspond to transitions $|g0\rangle \rightarrow |g1\rangle$ and $|e0\rangle \rightarrow |e1\rangle$, where “ g ” and “ e ” denote, respectively, the ground and excited states of the qubit, and “0” and “1” the number of photons in the oscillator's Fock state. Avoided level crossings between the qubit and oscillator transition signals are also observed

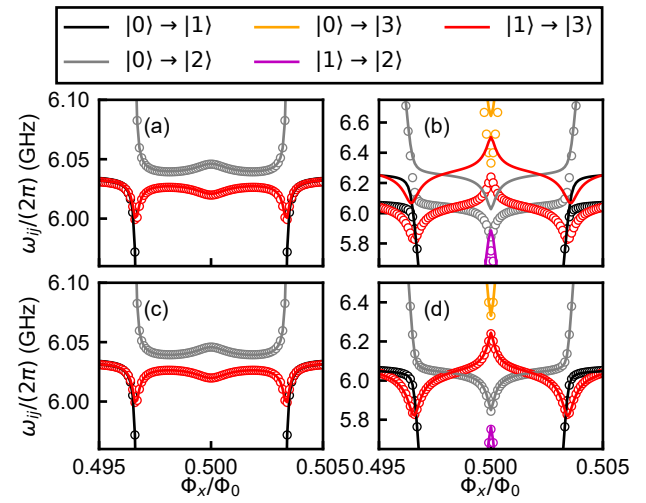


FIG. 4. Transition frequencies of the qubit-oscillator circuit for (a), (c) $L_c = 20$ pH and (b), (d) $L_c = 350$ pH. (a), (b) Numerically calculated transition frequencies from $\hat{\mathcal{H}}_{circ}$ are plotted as circles, while the transition frequencies of $\hat{\mathcal{H}}_R$ are plotted as lines. The parameters of $\hat{\mathcal{H}}_R$ obtained from $\hat{\mathcal{H}}_{circ}$ by mapping the lowest two levels of $\hat{\mathcal{H}}_2$ to the qubit are $\omega/(2\pi) = 6.033$ GHz, $\Delta_q/(2\pi) = 1.240$ GHz, $g/(2\pi) = 0.424$ GHz, and $I_p = 281.3$ nA for $L_c = 20$ pH and $\omega/(2\pi) = 6.272$ GHz, $\Delta_q/(2\pi) = 2.139$ GHz, $g/(2\pi) = 7.338$ GHz, and $I_p = 282.5$ nA for $L_c = 350$ pH. (c), (d) Numerically calculated transition frequencies from $\hat{\mathcal{H}}_{circ}$ are plotted as circles, while the results of the fitting by $\hat{\mathcal{H}}_R$ are plotted as lines. The parameters of $\hat{\mathcal{H}}_R$ obtained by fitting the spectra of $\hat{\mathcal{H}}_{circ}$ to $\hat{\mathcal{H}}_R$ are $\omega/(2\pi) = 6.033$ GHz, $\Delta_q/(2\pi) = 1.240$ GHz, $g/(2\pi) = 0.430$ GHz, and $I_p = 281.3$ nA for $L_c = 20$ pH and $\omega/(2\pi) = 6.064$ GHz, $\Delta_q/(2\pi) = 2.388$ GHz, $g/(2\pi) = 7.822$ GHz, and $I_p = 282.9$ nA for $L_c = 350$ pH. Black, gray, orange, magenta, and red colors indicate transitions $|0\rangle \rightarrow |1\rangle$, $|0\rangle \rightarrow |2\rangle$, $|0\rangle \rightarrow |3\rangle$, $|1\rangle \rightarrow |2\rangle$, and $|1\rangle \rightarrow |3\rangle$, respectively.

approximately at $\Phi_x/\Phi_0 = 0.497$ and 0.503 . In the case $L_c = 350$ pH, the characteristic spectrum indicates that the qubit-oscillator circuit is in the deep-strong-coupling regime [15]. Transition frequencies of $\hat{\mathcal{H}}_R$ are also plotted in Figs. 4(a) and (b). It should be mentioned that the parameters of $\hat{\mathcal{H}}_R$ are obtained in two different ways. Here, the parameters of $\hat{\mathcal{H}}_R$ are obtained from $\hat{\mathcal{H}}_{circ}$ by mapping the lowest two levels of $\hat{\mathcal{H}}_2$ to the qubit. The overall shapes of the spectra of $\hat{\mathcal{H}}_R$ and $\hat{\mathcal{H}}_{circ}$ look similar. On the other hand, the shift of the entire spectrum becomes as large as more than 200 MHz for $L_c = 350$ pH. To quantify the difference of the spectra between $\hat{\mathcal{H}}_R$ and $\hat{\mathcal{H}}_{circ}$, transition frequencies up to the third excited state numerically calculated from $\hat{\mathcal{H}}_{circ}$ are fitted by $\hat{\mathcal{H}}_R$. Figures 4(c) and (d) show that the same spectra of $\hat{\mathcal{H}}_{circ}$ in Figs. 4(a) and (b) are well fitted by $\hat{\mathcal{H}}_R$, but with a different parameter set.

Figure 5 shows parameters of $\hat{\mathcal{H}}_R$ obtained from $\hat{\mathcal{H}}_{circ}$ by mapping the lowest two energy levels of $\hat{\mathcal{H}}_2$ to the qubit and by fitting the spectra of $\hat{\mathcal{H}}_{circ}$ up to the third

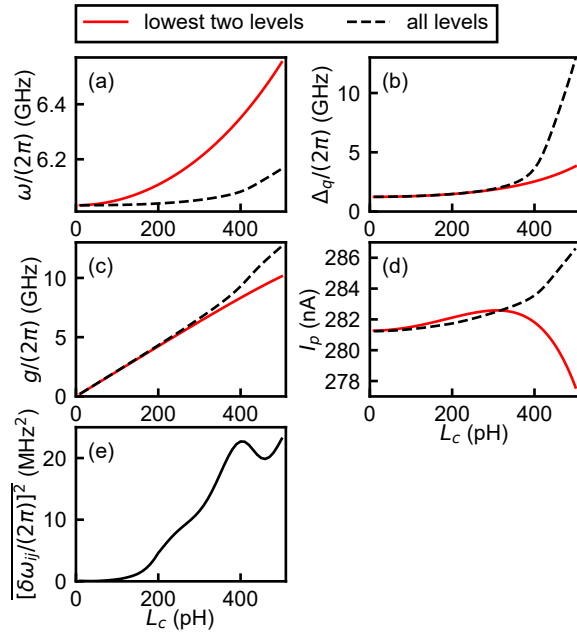


FIG. 5. Parameters of $\hat{\mathcal{H}}_R$ obtained from $\hat{\mathcal{H}}_{circ}$ by mapping the lowest two energy levels of $\hat{\mathcal{H}}_2$ to the qubit (red solid lines) and by fitting the spectra of $\hat{\mathcal{H}}_{circ}$ up to the third excited state to $\hat{\mathcal{H}}_R$ (black dashed lines) as a function of L_c . Panels (a)-(d) respectively correspond to the oscillator frequency ω , qubit frequency Δ_q , coupling strength g , and persistent current I_p in $\hat{\mathcal{H}}_R$. (e) The average of the squares of the residuals in the least-squares method of obtaining the parameters of $\hat{\mathcal{H}}_R$ by fitting, $[\delta\omega_{0i}/(2\pi)]^2$ ($i = 1, 2$, and 3).

excited state to $\hat{\mathcal{H}}_R$ as a function of L_c . The parameters of $\hat{\mathcal{H}}_R$ obtained in these two different ways become quite different from each other at large values of L_c due to contributions of the qubit's higher energy levels. On the other hand, the average of the squares of the residuals in the least-squares method of obtaining the parameters of $\hat{\mathcal{H}}_R$ by fitting, $[\delta\omega_{0i}/(2\pi)]^2$ ($i = 1, 2$, and 3), remains at the moderate level, at most 25 MHz 2 , which is consistent with the good fitting shown in Figs. 4(c) and (d). In fact, the energy level structure of $\hat{\mathcal{H}}_{circ}$ up to the seventh excited state can still be fitted well by the quantum Rabi Hamiltonian as shown in Appendix B.

One of the most paradoxical features of $\hat{\mathcal{H}}_R$ in the deep-strong-coupling regime is the non-negligible expectation number of photons in the oscillator in the ground state. In the case of the circuit shown in Fig. 1(a), the expectation number of photons can be investigated using the operator $\hat{\mathcal{H}}_1/(\hbar\omega) - 0.5$ in $\hat{\mathcal{H}}_{circ}$, which corresponds to $\hat{a}^\dagger\hat{a}$ in $\hat{\mathcal{H}}_R$. As shown in Fig. 6(a), a non-negligible expectation number of photons in the oscillator is obtained. Another paradoxical feature of $\hat{\mathcal{H}}_R$ in the deep-strong-coupling regime is a non-negligible expectation value of the field operator $\langle \hat{a} + \hat{a}^\dagger \rangle$ when the qubit flux bias is $\Phi_x \neq 0.5\Phi_0$. The expectation value of the field operator can also be investigated using the operator $\hat{\Phi}_1/(L_{LC}I_{zpf})$

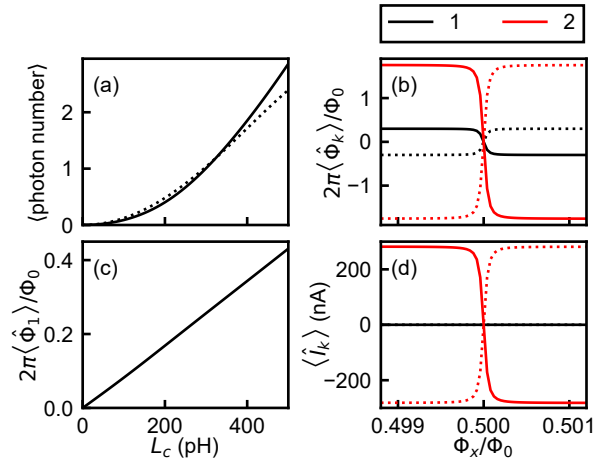


FIG. 6. (a) Expectation numbers of photons in the oscillator in the ground state as a function of L_c . The solid curve corresponds to $\langle 0 | \hat{\mathcal{H}}_1 | 0 \rangle / (\hbar\omega) - 0.5$, while the dashed line indicates the simple expression $(g/\omega)^2$, which is true in the limit $\Delta_q \ll \omega$. (b) [(d)] Expectation values of fluxes $2\pi\langle\hat{\Phi}_k\rangle/\Phi_0$ [Expectation values of currents $\langle\hat{I}_k\rangle$] as functions of the flux bias Φ_x in the case $L_c = 350$ pH. Black and red colors respectively indicate $k = 1$ and 2, and solid and dashed lines indicate the ground and the excited states, respectively. (c) Expectation value of flux $2\pi\langle\hat{\Phi}_1\rangle/\Phi_0$ in the ground state as a function of L_c at $\Phi_x/\Phi_0 = 0.498$.

in $\hat{\mathcal{H}}_{circ}$, which corresponds to $\hat{a} + \hat{a}^\dagger$ in $\hat{\mathcal{H}}_R$. Fig. 6(b) shows the expectation value of fluxes, $\langle\hat{\Phi}_1\rangle$ and $\langle\hat{\Phi}_2\rangle$, as functions of the flux bias Φ_x for the ground and the first excited states in the case $L_c = 350$ pH. At $\Phi_x/\Phi_0 \neq 0.5$, a nonzero expectation value $\langle\hat{\Phi}_1\rangle$ is demonstrated. One may suspect that a nonzero $\langle\hat{\Phi}_1\rangle$ is unphysical because it might result in a nonzero DC current through the inductor of an LC oscillator in the energy eigenstate. The relation between the flux and current operators is explicitly given in the circuit model:

$$\begin{pmatrix} L_c + L_1 & L_c \\ L_c & L_c + L_2 \end{pmatrix} \begin{pmatrix} \hat{I}_1 \\ \hat{I}_2 \end{pmatrix} = \begin{pmatrix} \hat{\Phi}_1 \\ \hat{\Phi}_2 \end{pmatrix}, \quad (7)$$

where \hat{I}_k ($k = 1, 2$) is defined as the operator of the current flowing from the ground node to node k . Note that in the case $L_c = 0$, $\hat{I}_1 = \hat{\Phi}_1/L_1$ and $\hat{I}_2 = \hat{\Phi}_2/L_2$. As shown in Fig. 6(c), at $\Phi_x/\Phi_0 = 0.498$, the expectation value $2\pi\langle\hat{\Phi}_1\rangle/\Phi_0$ in the ground state linearly increases as L_c , and is zero when $L_c = 0$. Fig. 6(d) shows the expectation values of currents $\langle\hat{I}_1\rangle$ and $\langle\hat{I}_2\rangle$ as functions of Φ_x in the case $L_c = 350$ pH. The expectation values $\langle\hat{I}_2\rangle$ are nonzero at $\Phi_x/\Phi_0 \neq 0.5$, while $\langle\hat{I}_1\rangle$ are exactly zero at all values of Φ_x . In this way, although $\langle\hat{\Phi}_1\rangle$ are

nonzero in the case $L_c \neq 0$, an unphysical DC current through the inductor of an LC oscillator is not predicted.

In conclusion, we have derived the Hamiltonian of a superconducting circuit that comprises a single-Josephson-junction flux qubit and an LC oscillator using the standard quantization procedure. Excluding the qubit's higher energy levels, the derived circuit Hamiltonian takes the form of the quantum Rabi Hamiltonian. The qubit's higher energy levels mainly cause a negative shift of the entire spectrum, but the energy level structure can still be fitted well by the quantum Rabi Hamiltonian even when the qubit-oscillator circuit is in the deep-strong-coupling regime. We found that some of the paradoxical properties of the quantum Rabi Hamiltonian, the non-negligible expectation number of photons and expectation value of the flux operator in the oscillator in the ground state, also arise from the circuit Hamiltonian.

ACKNOWLEDGMENTS

We are grateful to M. Devoret for valuable discussions. This work was supported by Japan Society for the Promotion of Science (JSPS) Grants-in-Aid for Scientific Research (KAKENHI) (No. JP19H01831), Japan Science and Technology Agency (JST) Precursory Research for Embryonic Science and Technology (PRESTO) (Grant No. JPMJPR1767), and JST Core Research for Evolutionary Science and Technology (CREST) (Grant No. JPMJCR1775).

Appendix A: Numerical calculation method

As a simple example, let us consider $\hat{\mathcal{H}}_1$ in the main text:

$$\begin{aligned}\hat{\mathcal{H}}_1 &= \frac{\hat{q}_1^2}{2C} + \frac{\hat{\Phi}_1^2}{2L_{LC}} \\ &= 4E_C\hat{n}^2 + \frac{1}{2}E_L\hat{\phi}^2,\end{aligned}\quad (\text{A1})$$

where, $E_C = e^2/(2C)$, $E_L = [\Phi_0/(2\pi)]^2/L_{LC}$, and $\hat{\phi}$ and \hat{n} are operators of dimensionless magnetic flux and charge, respectively, and satisfy $[\hat{\phi}, \hat{n}] = i$. Using the relation $\hat{\phi} = -(1/i)\partial/\partial n$, the Hamiltonian is rewritten as

$$\hat{\mathcal{H}}_1 = 4E_C\hat{n}^2 - \frac{1}{2}E_L\frac{\partial^2}{\partial n^2}. \quad (\text{A2})$$

Let us calculate wavefunctions $\psi(n)$ and their eigenenergies E of this Hamiltonian. We expand the wavefunction with the plane waves as

$$\psi(n) = \sum_k \psi_k \frac{e^{ikn}}{\sqrt{2n_{max}}}. \quad (\text{A3})$$

Here, $2n_{max}$ is the length of the n -space. Considering the periodic boundary condition $\psi(-n_{max}) = \psi(n_{max})$, the wave number k is given by

$$k = \frac{2\pi}{2n_{max}}\eta, (\eta = 0, \pm 1, \pm 2, \dots). \quad (\text{A4})$$

Then, the equation for determining ψ_k and E is obtained as

$$\begin{aligned}\hat{\mathcal{H}}_1\psi(n) &= E\psi(n) \\ \sum_{k'} \left[4E_Cn^2 + \frac{1}{2}E_Lk'^2 \right] \psi_{k'} \frac{e^{ik'n}}{2n_{max}} &= E \sum_{k'} \psi_{k'} \frac{e^{ik'n}}{2n_{max}} \\ \int_{-n_{max}}^{n_{max}} dn \frac{e^{-ikn}}{\sqrt{2n_{max}}} \sum_{k'} \left[4E_Cn^2 + \frac{1}{2}E_Lk'^2 \right] \psi_{k'} \frac{e^{ik'n}}{2n_{max}} &= \int_{-n_{max}}^{n_{max}} dn \frac{e^{-ikn}}{\sqrt{2n_{max}}} E \sum_{k'} \psi_{k'} \frac{e^{ik'n}}{2n_{max}} \\ \sum_{k'} \left[4E_C f_{k-k'}(n^2) + \delta_{k,k'} \frac{1}{2}E_Lk^2 \right] \psi_{k'} &= E\psi_k,\end{aligned}\quad (\text{A5})$$

where

$$f_{k-k'}(n^2) \equiv \frac{1}{2n_{max}} \int_{-n_{max}}^{n_{max}} dn e^{-i(k-k')n} n^2. \quad (\text{A6})$$

The set of wavefunctions and eigenenergies are obtained

by solving Eq. (A5). Numerically, we can get $f_{k-k'}(n^2)$ by the fast Fourier transform (FFT) for discretized n -space. After solving the eigenvalue equation in Eq. (A5), the wavefunctions $\psi(n)$ are also obtained from ψ_k by the FFT. For the calculation of $\hat{\mathcal{H}}_2$ in the main text, we use the following equation instead of Eq. (A5),

$$\sum_{k'} \left\{ 4E_C J f_{k-k'}(n^2) + \delta_{k,k'} \left[-E_J \cos(k - k_x) + \frac{1}{2}E_{LFQ}k^2 \right] \right\} \psi_{k'} = E\psi_k, \quad (\text{A7})$$

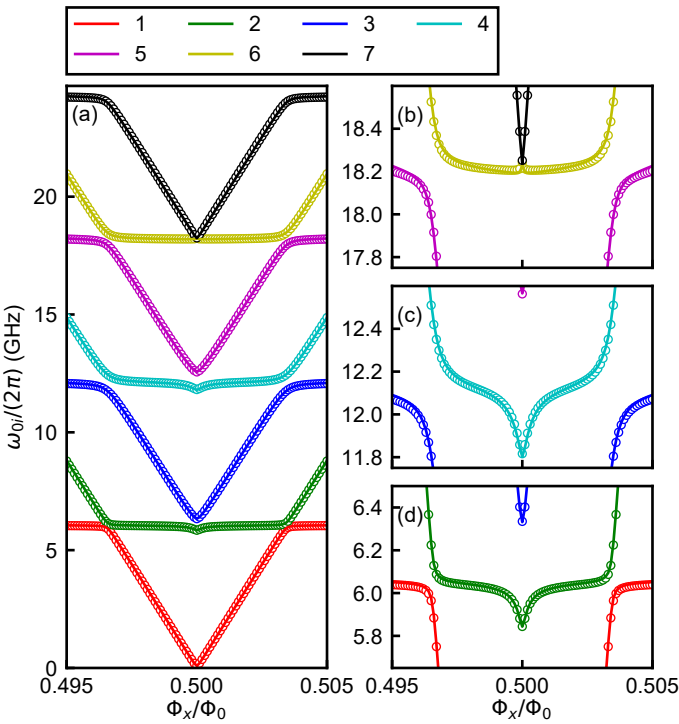


FIG. 7. (a) Transition frequencies of the qubit-oscillator circuit up to the seventh excited state for $L_c = 350$ pH. Numerically calculated transition frequencies from \mathcal{H}_{circ} are plotted as circles, while the results of the fitting by \mathcal{H}_R are plotted as lines. The parameters of \mathcal{H}_R obtained by fitting the spectra of \mathcal{H}_{circ} to \mathcal{H}_R are $\omega/(2\pi) = 6.054$ GHz, $\Delta_q/(2\pi) = 2.133$ GHz, $g/(2\pi) = 7.562$ GHz, and $I_p = 282.2$ nA. Red, green, blue, cyan, magenta, yellow, and black colors indicate transition frequencies ω_{01} , ω_{02} , ω_{03} , ω_{04} , ω_{05} , ω_{06} , and ω_{07} , respectively. (b), (c), (d) The same spectra with smaller range of frequency around 3ω , 2ω , and ω .

where $E_{CJ} = e^2/(2C_J)$, $E_{LFQ} = [\Phi_0/(2\pi)]^2/L_{FQ}$, and $k_x = 2\pi\Phi_x/\Phi_0$.

Appendix B: Fitting of \mathcal{H}_{circ} up to the seventh excited state

Transition frequencies of the qubit-oscillator circuit numerically calculated from \mathcal{H}_{circ} up to the seventh excited state are plotted in Figure 7 for $L_c = 350$ pH. The calculated spectra can still be fitted well by \mathcal{H}_R . The average of the squares of the residuals in the least-squares method of obtaining the parameters of \mathcal{H}_R by fitting, $[\delta\omega_{0i}/(2\pi)]^2$ ($i = 1, 2, 3, 4, 5, 6$, and 7), is 152 MHz². This value is almost 10 times larger than the case of the fitting up to the third excited state, but still within a moderate level considering that the largest transition frequency is more than 20 GHz.

[1] Y. Nakamura, Y. A. Pashkin, and J. S. Tsai, *Nature* **398**, 786 (1999).
[2] U. Vool and M. Devoret, *International Journal of Circuit Theory and Applications* **45**, 897 (2017).
[3] Y. Nakamura, C. D. Chen, and J. S. Tsai, *Phys. Rev. Lett.* **79**, 2328 (1997).
[4] T. P. Orlando, J. E. Mooij, L. Tian, C. H. van der Wal, L. S. Levitov, S. Lloyd, and J. J. Mazo, *Phys. Rev. B* **60**, 15398 (1999).
[5] D. Vion, A. Aassime, A. Cottet, P. Joyez, H. Pothier, C. Urbina, D. Esteve, and M. H. Devoret, *Science* **296**, 886 (2002).
[6] J. M. Martinis, S. Nam, J. Aumentado, and C. Urbina, *Physical review letters* **89**, 117901 (2002).
[7] J. Koch, T. M. Yu, J. Gambetta, A. A. Houck, D. I. Schuster, J. Majer, A. Blais, M. H. Devoret, S. M. Girvin, and R. J. Schoelkopf, *Phys. Rev. A* **76**, 042319 (2007).
[8] Y. A. Pashkin, T. Yamamoto, O. Astafiev, Y. Nakamura, D. Averin, and J. S. Tsai, *Nature* **421**, 823 (2003).
[9] I. Chiorescu, P. Bertet, K. Semba, Y. Nakamura, C. J. P. M. Harmans, and J. E. Mooij, *Nature* **431**, 159 (2004).
[10] A. Blais, R.-S. Huang, A. Wallraff, S. M. Girvin, and R. J. Schoelkopf, *Phys. Rev. A* **69**, 062320 (2004).
[11] A. O. Niskanen, K. Harrabi, F. Yoshihara, Y. Nakamura, and J. S. Tsai, *Phys. Rev. B* **74**, 220503(R) (2006).
[12] T. Niemczyk, F. Deppe, H. Huebl, E. P. Menzel, F. Hocke, M. J. Schwarz, J. J. Garcia-Ripoll, D. Zueco, T. Hümmer, E. Solano, A. Marx, and R. Gross, *Nat. Phys.* **6**, 772 (2010).
[13] P. Forn-Díaz, J. Lisenfeld, D. Marcos, J. J. Garcia-Ripoll, E. Solano, C. J. P. M. Harmans, and J. E. Mooij, *Phys. Rev. Lett.* **105**, 237001 (2010).
[14] F. Yoshihara, T. Fuse, S. Ashhab, K. Kakuyanagi, S. Saito, and K. Semba, *Nat. Phys.* **13**, 44 (2017).
[15] F. Yoshihara, T. Fuse, S. Ashhab, K. Kakuyanagi, S. Saito, and K. Semba, *Phys. Rev. A* **95**, 053824 (2017).
[16] F. Yoshihara, T. Fuse, Z. Ao, S. Ashhab, K. Kakuyanagi, S. Saito, T. Aoki, K. Koshino, and K. Semba, *Phys. Rev. Lett.* **120**, 183601 (2018).
[17] I. I. Rabi, *Phys. Rev.* **51**, 652 (1937).

- [18] E. T. Jaynes and F. W. Cummings, Proc. IEEE **51**, 89 (1963).
- [19] D. Braak, Phys. Rev. Lett. **107**, 100401 (2011).
- [20] J. Bourassa, J. M. Gambetta, A. A. Abdumalikov Jr, O. Astafiev, Y. Nakamura, and A. Blais, Physical Review A **80**, 032109 (2009).
- [21] B. Peropadre, D. Zueco, D. Porras, and J. J. García-Ripoll, Phys. Rev. Lett. **111**, 243602 (2013).
- [22] W. C. Smith, A. Kou, U. Vool, I. M. Pop, L. Frunzio, R. J. Schoelkopf, and M. H. Devoret, Phys. Rev. B **94**, 144507 (2016).
- [23] J. Peltonen, P. Coumou, Z. Peng, T. Klapwijk, J. S. Tsai, and O. Astafiev, Scientific reports **8**, 1 (2018).
- [24] T. M. Hazard, A. Gyenis, A. Di Paolo, A. T. Asfaw, S. A. Lyon, A. Blais, and A. A. Houck, Phys. Rev. Lett. **122**, 010504 (2019).
- [25] L. Grünhaupt, M. Spiecker, D. Gusekova, N. Maleeva, S. T. Skacel, I. Takmakov, F. Valenti, P. Winkel, H. Rotzinger, W. Wernsdorfer, et al., Nature materials **18**, 816 (2019).
- [26] V. E. Manucharyan, J. Koch, L. I. Glazman, and M. H. Devoret, **326**, 113 (2009).
- [27] S. Ashhab and F. Nori, Phys. Rev. A **81**, 042311 (2010).
- [28] A. Stokes and A. Nazir, Nature communications **10**, 1 (2019).
- [29] M. Roth, F. Hassler, and D. P. DiVincenzo, Physical Review Research **1**, 033128 (2019).
- [30] O. Di Stefano, A. Settineri, V. Macrì, L. Garziano, R. Stassi, S. Savasta, and F. Nori, Nature Physics **15**, 803 (2019).
- [31] J. R. Johansson, P. D. Nation, and F. Nori, Comp. Phys. Commun. **184**, 1234 (2013).